Article ID: 1003－6326(2004)02－0291－06

Phase-field simulations of solidification of Al-Cu binary alloys①

LONG Wen-yuan(龙文元), CAI Qi-zhou(蔡启舟), CHEN Li-liang(陈立亮), WEI Bo-kang(魏伯康)
(State Key Laboratory of Die Technology, Huazhong University of Science and Technology, Wuhan 430074, China)

Abstract: The dendrite growth process during the solidification of the Al-4.5% Cu binary alloy was simulated using the phase-field model, proposed by Kim et al. Solute diffusion equation and heat transfer equation were solved simultaneously. The effects of the noise on the dendrite growth, solute and temperature profile in the undercooled alloy melt were investigated. The results indicate that the noise can trigger the growth of the secondary arms, and increase the highest temperature and solute concentration, but not influence the tip operating state. The solute and temperature gradients in the tip are the highest.

Key words: Al-Cu alloy; phase-field model; dendrite growth; solute profile; temperature profile
CLC number: TG 248 **Document code:** A

1 INTRODUCTION

In recent years the phase-field method has been extensively used for simulations of dendrite growth. Phase-field method is expected a powerful tool for describing complex phase transitions in non-equilibrium state. In the phase-field method a new variable φ is introduced to indicate the physical state of the system at each point. The phase-field model is based on the Ginzburg-Landau or Cahn-Hilliard type of free energy function, and the solution of equation can be used to describe the complicated morphologies of dendritic growth without explicitly tracking the complex free boundaries.

Kobayashi[1] developed a phase-field involving anisotropy for simulating the dendrite growth in the undercooled melt of pure material. For evaluating the reliability and accuracy of the phase-field, Wheeler et al[2-4] used this model to compute dendrite growth speeds and compared them with the predictions of solvability theory. Karma et al[5, 6] used the thin interface limit phase field to 2D and 3D dendrite growth in the solidification of pure metal quantitatively. The results agree well with the solvability theory. Charach, Beckermann and Tong et al[7-9] investigated the effect of melt convection on the dendrite growth in pure material solidification by using the phase-field.

The first phase-field model for alloys was developed by Wheeler et al[10] (WBM model) in a thermodynamically consistent way. In this model, the mixture of solid and liquid both with the same composition is assumed in the interface region. The phase-field parameters are determined not only in a sharp interface limit, but also in a finite interface thickness limit. The model has been used by the original authors[11-13] to study solute trapping and the recalescence.

Recently, Kim et al[14] have proposed a new phase-field model for binary alloys (KKS model). The model is equivalent with the WBM model, but it has a different definition of the free energy density for the interfacial region. The limit of the interface width in the WBM model disappears. The model has been used by the original authors to study the microstructure evolution during the rapid solidification of Fe-C, Fe-C-P and Al-Si alloys[14-19]. Seol et al[20] developed the high temperature stress model for continuously cast steels based on this model, and studied the effect of the dendritic morphology on the mechanical strength of carbon steels.

In the present paper, we adopt KKS model[14-19] to study the dendrite growth in solidification of Al-Cu alloys, and use a vanishing kinetic coefficient. The concentration and temperature equations are solved simultaneously.

2 GOVERNING EQUATIONS

2.1 Phase-field equation

In the phase-field model, the state of the phase is represented continuously by an order parameter, the phase-field, φ. For example, $\varphi = 1$, $\varphi = 0$ and a finite region in which $0 < \varphi < 1$ represent solid, liquid and the interface respectively. The time change of the phase-field is assumed to be proportional to the varia-

① **Foundation item:** Project (10176009) supported by the National Natural Science Foundation of China
Received date: 2003－05－30; **Accepted date:** 2003－09－20
Correspondence: LONG Wen-yuan, PhD candidate; Tel: +86-27-87543876; E-mail: long_weny@sohu.com

tion of the free energy functional.

$$\frac{\partial \varphi}{\partial t} = M \frac{\delta F}{\delta \varphi} \tag{1}$$

where M is the phase-field mobility which is related to the driving force for the interface. The Helmholtz free energy functional F has the form:

$$F = \int_V \left| \frac{1}{2} \varepsilon^2 | \nabla \varphi |^2 + f(\varphi, T) \right| \mathrm{d}V \tag{2}$$

In KKS model, the free energy density is the sum of the free energies of solid, liquid and a double-well potential in the interface region. The free energy density is expressed as

$$f(\varphi, T) = h(\varphi) f^{\mathrm{S}}(c_{\mathrm{S}}) + (1 - h(\varphi)) \cdot f^{\mathrm{L}}(c_{\mathrm{L}}) + Wg(\varphi) \tag{3}$$

$$h(\varphi) = \varphi^3 (10 - 15\varphi + 6\varphi^2) \tag{4}$$

$$g(\varphi) = \varphi^2 (1 - \varphi)^2 \tag{5}$$

where $h(\varphi)$ is the potential function, $g(\varphi)$ is the double-well potential, W is the height of the double-well potential, $f^{\mathrm{S}}(c_{\mathrm{S}})$ and $f^{\mathrm{L}}(c_{\mathrm{L}})$ are the free energies of the solid and liquid phases respectively.

For a dilute alloy, the detailed equation of the phase-field is given by

$$\frac{\partial \varphi}{\partial t} = M \left| \varepsilon^2(\theta) \nabla^2 \varphi + \frac{RT}{V_{\mathrm{m}}} h'(\varphi) \cdot \ln \frac{(1 - c_{\mathrm{S}}^{\mathrm{e}})(1 - c_{\mathrm{L}})}{(1 - c_{\mathrm{L}}^{\mathrm{e}})(1 - c_{\mathrm{s}})} - Wg'(\varphi) \right| \tag{6}$$

where ε is the phase-field parameter, R is the gas constant, T is the temperature, V_{m} is the molar volume, and c is the solute composition; the superscript e shows equilibrium state, the subscripts S and L show solid and liquid phases respectively.

Usually, the interface energy of metal has anisotropy, so the anisotropy is introduced in the phase-field parameter as follows:

$$\varepsilon(\theta) = \varepsilon(1 + v\cos(k\theta)) \tag{7}$$

where k is the mode number; v is the magnitude of anisotropy; θ is the angle between the direction of phase-field gradient and reference axis of the system, $\tan\theta = \varphi_x / \varphi_y$.

The phase-field parameter of ε and W are related to the interface energy, σ, and the interface width, 2λ. M is related to the kinetic coefficient, β. Then they are given by

$$\varepsilon = \sqrt{\frac{6\lambda}{2.2}}\sigma, \quad W = \frac{6.6\sigma}{\lambda} \tag{8}$$

$$M^{-1} = \frac{\varepsilon^2}{\sigma} \left| \frac{RT}{V_{\mathrm{m}}} \frac{1 - k_{\mathrm{e}}}{m_{\mathrm{e}}} \beta + \frac{\varepsilon}{D_{\mathrm{i}} \sqrt{2W}} \zeta(c_{\mathrm{S}}^{\mathrm{e}}, c_{\mathrm{L}}^{\mathrm{e}}) \right| \tag{9}$$

$$\zeta(c_{\mathrm{S}}^{\mathrm{e}}, c_{\mathrm{L}}^{\mathrm{e}}) = f_{\mathrm{cc}}^{\mathrm{S}}(c_{\mathrm{S}}^{\mathrm{e}}) f_{\mathrm{cc}}^{\mathrm{L}}(c_{\mathrm{L}}^{\mathrm{e}}) (c_{\mathrm{L}}^{\mathrm{e}} - c_{\mathrm{S}}^{\mathrm{e}})^2 \cdot \int_0 \frac{h(\varphi)(1 - h(\varphi))}{(1 - h(\varphi)) f_{\mathrm{cc}}^{\mathrm{s}}(c_{\mathrm{S}}^{\mathrm{e}}) + h(\varphi) f_{\mathrm{cc}}^{\mathrm{L}}(c_{\mathrm{L}}^{\mathrm{e}})} \cdot \frac{\mathrm{d}\varphi}{\varphi(1 - \varphi)} \tag{10}$$

where m_{e} is the equilibrium slope of the liquidus, k_{e} is the equilibrium partition coefficient, and D_{i} is the diffusion coefficient in the interface region.

2.2 Diffusion equation

The solute diffusion equation is given by:

$$\frac{\partial c}{\partial t} = \nabla \cdot \left[\frac{D(\varphi)}{f_{\mathrm{cc}}} \nabla f_{\mathrm{c}} \right] \tag{11}$$

where $D(\varphi)$ is the solute diffusion coefficient, subscripts f_{c} and f_{cc} stand for the first and second derivatives by corresponding variables.

The solute composition in the interface region is the fraction-weighted sum of solid and liquid compositions. The chemical potentials of solute and solvent are selected as a thermodynamic variable of constraint, and those of solid and liquid phases are assumed to be equal at any point within the interface region, i.e.

$$c = h(\varphi) c_{\mathrm{S}} + (1 - h(\varphi)) c_{\mathrm{L}} \tag{12}$$

$$\mu^{\mathrm{S}}(c_{\mathrm{S}}(x, t)) = \mu^{\mathrm{L}}(c_{\mathrm{L}}(x, t)) \tag{13}$$

The stochastic noise is needed to stimulate the fluctuations in the solid/liquid interface region, which gives rise to most structures observed in real systems. Here we have incorporated the concentration noise in the diffusion equation by a simple manner. Specifically, the noise can be introduced by modifying equation (11), i.e.

$$\partial c / \partial t \rightarrow \partial c / \partial t + 16 g(\varphi) \times \dot{\omega} \tag{14}$$

where $\times$ is a random number between − 1 and + 1, $\dot{\omega}$ gives the magnitude of the fluctuation. Note that the factor $16g(\varphi)$ has a maximum value of 1 at $\varphi = 0.5$ and drops off rapidly away from the interface.

2.3 Thermal diffusion equation

In this study, the temperature equation is solved simultaneously using a double grid method. Since the thermal diffusivity of Al-4.5% Cu alloy is about several hundred times larger than that of the solute, the grid size for temperature calculation is set to be ten times larger than that for the phase-field and concentration-field calculation in order to save the calculation time. The latent heat extraction is estimated by summing up the change of phase-field within the corresponding temperature grid, then the thermal diffusion equation is obtained as follows:

$$\rho c_p \frac{\partial T}{\partial t} = k \nabla^2 T + \Delta H \sum A h'(\varphi) \frac{\partial \varphi}{\partial t} \tag{15}$$

where k is the thermal conductivity, ΔH is the heat of fusion per volume, c_p is the specific heat capacity and A represents the area ratio of the phase-field grid to thermal one.

3 CALCULATIONS

In the calculation, Eqns. (6) and (11) were discretized on uniform grids using an explicit finite difference scheme. Eqn. (15) was numerically solved using an alternating direct implicit (ADI) method, which is unconditionally stable, irrespective of the

time step, Δt, employed. The Al-4. 5% Cu alloy is selected. The physical properties for Al-4. 5% Cu alloy used in calculation are shown in Table 1.

Table 1 Physical properties of Al-4. 5% Cu alloy

Physical properties	Value
Interface energy, $\sigma/(\mathrm{J}\cdot\mathrm{m}^{-2})$	0. 093
Melting point, T_m/K	933. 3
Solute diffusivity (liquid), $D_L/(\mathrm{m}^2\cdot\mathrm{s}^{-1})$	3.0×10^{-9}
Solute diffusivity (solid), $D_S/(\mathrm{m}^2\cdot\mathrm{s}^{-1})$	3.0×10^{-13}
Latent heat, $L/(\mathrm{kJ}\cdot\mathrm{kg}^{-1})$	389. 0
Slope of liquids, $m_e/(\mathrm{K}\cdot\mathrm{mol}\%^{-1})$	- 640. 0
Specific heat capacity, $c_p/(\mathrm{kJ}\cdot\mathrm{kg}^{-1}\cdot\mathrm{K}^{-1})$	1. 13
Thermal conductivity, $k/(\mathrm{W}\cdot\mathrm{m}^{-1}\cdot\mathrm{K}^{-1})$	192. 6
Equilibrium distribution coefficient, k_e	0. 14

The two dimension square calculation area of 750 × 750 grids for the phase-field and solute field and that of 75 × 75 grids for the thermal field are prepared. The grid sizes of the phase-field and the concentration field, and the thermal calculation are 1.0×10^{-8} m and 1.0×10^{-7} m respectively. A small triangle solid of 15 × 15 grids is initially put in the corner. The equations are solved with T = 900 K as initial temperature fixed on the boundary for the thermal equation. This is done in order to fit the non-isothermal temperature system to the isothermal case. The choice of Δt must be made in such a way that the equations remain stable under time-step iteration. For the diffusion equation in two dimensions it can be shown that $\Delta t < \Delta x^2/4D_L$ for stability, so a value of $\Delta t = \Delta x^2/5D_L$ has been selected in this study.

We only calculate the quarter of the dendrite because of the symmetry of the dendrite. The calculation is done in a computer of P4-1. 6GMHz.

4 RESULTS AND DISCUSSION

4. 1 Dendrite growth

The dendrite shapes of Al-4. 5% Cu alloy are shown in Fig. 1 for two different noise levels at time of 0. 16 ms. In Fig. 1(a) there is no noise($\dot{\omega}$= 0), the primary dendritic arms are very smooth, and there are no well-developed secondary arms. In Fig. 1 (b) the stochastic noise is imposed ($\dot{\omega}$= 0. 01), the dendrite has well-developed secondary arms, and the primary arms become finer. This result shows that the stochastic noise could trigger the growth of the secondary arms. The competitive growth of the secondary arms in the solidification is observed. The sidebranches begin their growth in a direction not perpendicular to the primary arm, but later, gradually develop a growth axis that is perpendicular to the primary arm. Behind the dendritic tip, the root of the side arm is significantly narrower than the body of the side arm. These features are commonly observed in real dendrites.

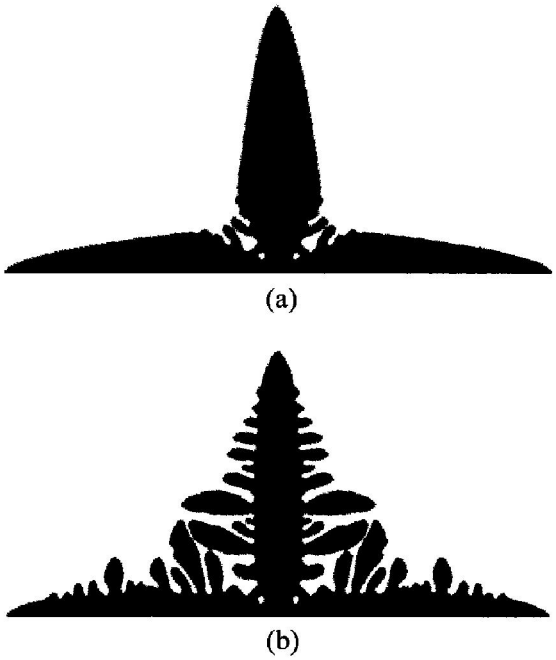

Fig. 1 Change in dendrite shape of Al-%4Cu alloy due to noise
(a) $\dot{\omega}$= 0; (b) $\dot{\omega}$= 0. 01

The tip position, speed and radius as a function of time are plotted in Figs. 2 - 4 respectively. Each figure shows the results for two different noise levels. The plots show that the tip position, speed and radius are very similar under two conditions. The results demonstrate that the concentration noise does not influence the tip operating state. The plots of the tip speed and radius show that the computed values of the tip speed and radius are of a little oscillatory, and the cooperation of the noise make the computed values tend to be a

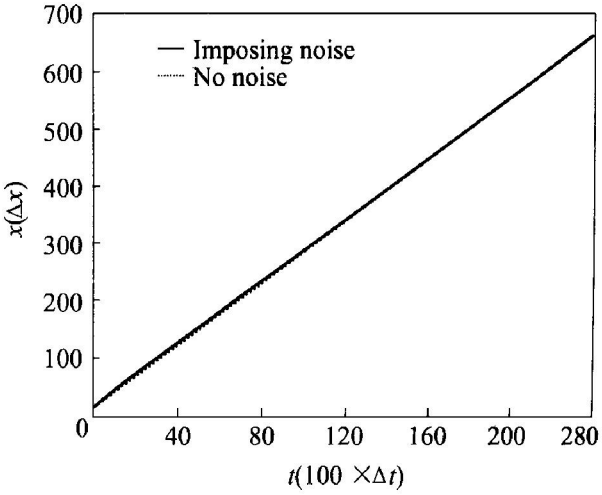

Fig. 2 Tip position versus time for dendrite growth

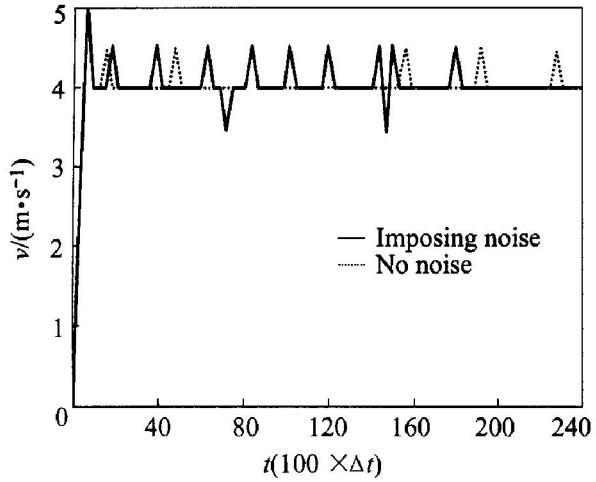

Fig. 3 Tip speed versus time for dendrite growth

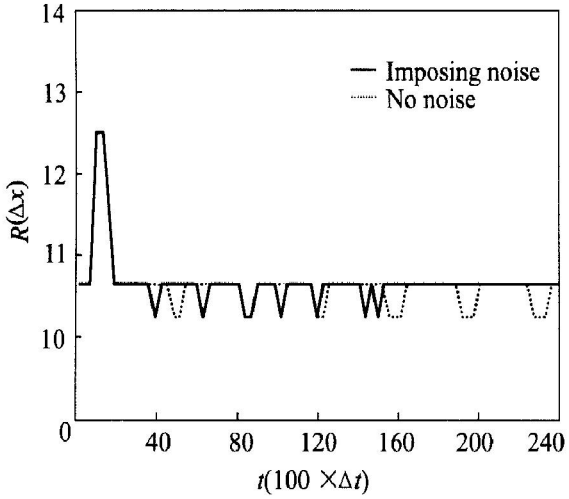

Fig. 4 Tip radius versus time for dendrite growth

constant.

It is noted here that using average values of the tip radius ($\overline{R}$ = 1.06 × 10^{-7}) and speed ($\overline{v}$ = 0.040 5), we obtain a value for the Peclet number, $\overline{Pe}$ = 0.718, where $\overline{Pe} = \overline{v}\,\overline{R}/2D_L$. The two-dimensional Ivantsov solution, which does not include capillarity or kinetics, yields Pe = 0.725 for ΔT = 33.3 K. This shows that the computed values agree well with Ivantsov theory.

4.2 Solute field

The concentration fields for Al-4.5% Cu alloy dendritically growing into a supercooled melt are shown in Fig. 5. The results show that the concentration profiles agree well with the dendrite growth.

Firstly, the spine of the primary arm has a low concentration, and the mushy regions between the dendritic secondary arms have the highest concentration. Secondly, the existence of spines of low concentration on the secondary arms that are as low as the spines of the primary arms. Thirdly, because the solute diffusivity is much less than the speed of the boundary transition, the solute, which precipitates

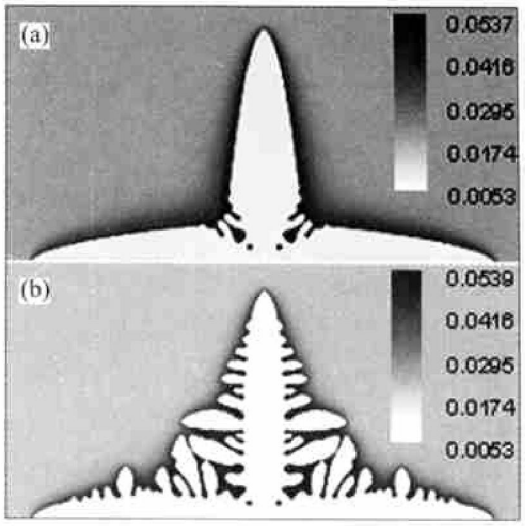

Fig. 5 Concentration field for dendrite growth at time 0.16 ms
a) —α= 0; (b) —α= 0.01

from the solid, does not diffuse in time, and the solute gradients form in the interface regions. The tip speed is the rapidest, therefore, the solute gradients existed in the interface before the dendritic tip is the highest, and that in the root of the primary arms is the smallest.

Fig. 6 shows the solute redistribution of the dendrite tip during the solidification. The results agree well with the solute redistributing theory in non-equilibrium state involving the diffusion in the solid and liquid.

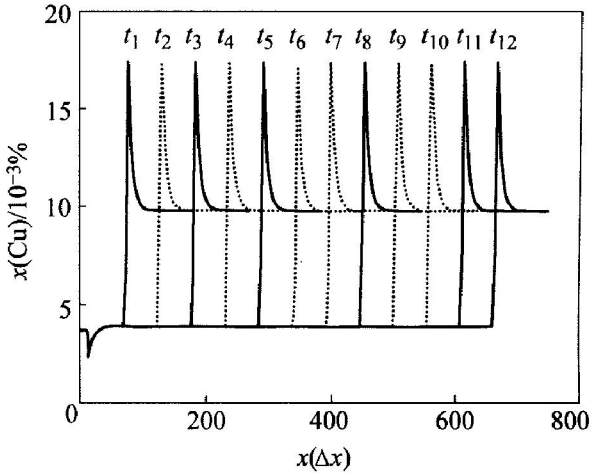

Fig. 6 Evolution of solute field in dendrite tip for different times

4.3 Temperature field

Fig. 7 demonstrates spatial redistribution of the temperature field for two different noise levels at time of 0.16 ms. The location of the hottest point during the crystal growth varies and in general corresponds to the tips of those secondary arms which grow towards each other and form a closed liquid pocket. Melt in this pocket is of the highest temperature due to the release of the latent heat by these growing sec-

ondary arms. The temperature does not vary much neither in time nor in space, and the spatial temperature difference does not exceed 0.4 K (Fig. 8).

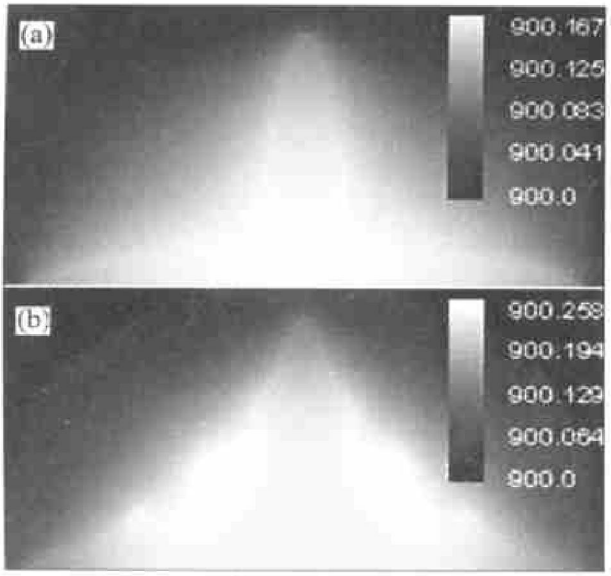

Fig. 7 Temperature field for dendrite growth at time of 0.16 ms
(a) —α= 0; (b) —α= 0.01

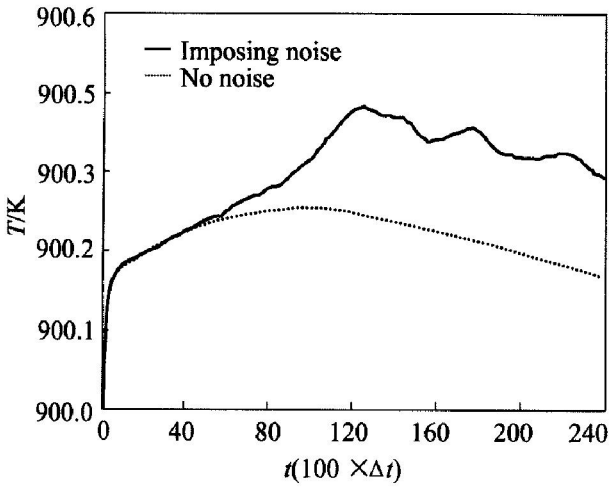

Fig. 8 Maximal temperature of system versus time (Minimal temperature T = 900 K is kept on the boundary all the time)

The maximal value of the system temperature as a function of time are shown in Fig. 8. Each figure shows the results for two different noise levels. The curve of imposing noise is slightly oscillatory because the temperature is taken at different grid points wherever the maximum value occurs. The local peaks occur when two or more sidebranches growing towards each other merge and stop growing and consequently produce the latent heat. Then another sidebranch surrounded by hot melt starts to release more latent heat than the others and becomes the hottest place in the system. This reflects the change of the temperature gradient owing to the release of latent heat. The curve with no noise is smooth, and the maximal value is less than that of imposing noise. This is because the stochastic noise could trigger the dendritic growth, then release more latent heat.

5 CONCLUSIONS

1) The dendrite growing morphologies could be simulated by using the phase-field method realistically, the growth of the secondary arms could be simulated by incorporating the concentration noise.

2) The noise could trigger the growth of the secondary arms, and increase the highest temperature in solid; but not influence the tip operating state. The computed value of Pelect number agrees well with the Ivantsov solution. The temperature gradients in the tip are the highest.

3) The spine of the primary arm has a low concentration, and the mushy regions between the dendritic secondary arms have the highest concentration. The solute gradients exist in the interface before the dendrite tip is the highest.

4) The results of simulation agree well with the features commonly observed in real solidification of binary alloy.

REFERENCES

[1] Kobayashi R. Modeling and numerical simulations of dendritic crystal growth[J]. Physica D, 1993, 63(3-4): 410.

[2] Wheeler A A, Murrary B T, Schaefer R J. Computation of dendrites using a phase field model[J]. Physica D, 1993, 66(1-2): 243.

[3] Wang S L, Sekerka R F, Wheeler A A, et al. Thermodynamically consistent phase-field models for solidification [J]. Physica D, 1993, 69(1-2): 189.

[4] Murray B T, Wheeler A A, Glicksman M E. Simulations of experimentally observed dendritic growth behavior using a phase-field model[J]. J Crystal Growth, 1995, 154(3-4): 386.

[5] Karma A, Rappel W J. Phase-field method for computationally efficient modeling of solidification with arbitrary interface kinetics[J]. Physical Review E, 1996, 53(4): 3017.

[6] Karma A, Rappel W J. Phase-field simulation of three-dimensional dendritic: is microscopic solvability theory correct? [J]. J Crystal Growth, 1997, 174(1-4): 54.

[7] Charach Ch, Fife P C. Phase-field models of solidification in binary alloys: capillarity and solute trapping effects [J]. J Crystal Growth, 1999, 198/199(2): 1267.

[8] Tong X, Beckermann C, Karma A. Velocity and shape selection of dendritic crystals in a forced flow[J]. Physical Rev E, 2000, 61(1): 49.

[9] Beckermann C, Li Q, Tong X. Microstructure evolution of equiaxed dendritic growth [J]. Sci Technol Adv Mater, 2001(2): 117.

[10] Wheeler A A, Boettinger W J, McFadden G B. Phase-field model for isothermal phase transitions in binary al-

loys[J]. Phys Rev A, 1992, 45(10): 7424.
[11] Wheeler A A, Ahmad N A. Boettinger W. J. Recent developments in the phase-field model of solidification [J]. Adv Space Res, 1995, 16(7): 163.
[12] Warren J A, Boettinger W J. Prediction of dendritic growth and microsegregation patterns in a binary alloy using the phase-field method[J]. Acta Metall Mater, 1995, 43(2): 689.
[13] Boettinger W J, Warren J A. The Phase-field method: simulation of alloy dendritic solidification during recalescence[J]. Metall Mater Trans A, 1996, 27A(3): 657.
[14] Kim S G, Kim W T, Suzuki T. Phase-field model for binary alloys[J]. Phys Rev E, 1999, 60(6): 7186.
[15] Kim S G, Kim W T. Phase-field modeling of rapid solidification[J]. Mater Sci Eng, 2001, A304-306(1-2): 281.
[16] Ode M, Suzuki T. Numerical simulation of initial microstructure evolution of Fe-C alloys using a phase-field model[J]. ISIJ International, 2002, 42(4): 368.
[17] Ode M, Suzuki T, Kim S G, et al. Phase-field model for solidification of Fe-C alloys[J]. Sci Technol Adv Mater, 2000(1): 43.
[18] Suzuki T, Ode M, Kim S G, et al. Phase-field model of dendritic growth[J]. J Crystal Growth, 2002, 237-239(1-41): 125.
[19] Ode M, Kim S G, Kim W T, et al. Numerical prediction of the secondary dendrite arm spacing using a phase-field model[J]. ISIJ International, 2001, 41(4): 345.
[20] Seol D J, Oh K H, Cho J W, et al. Phase-field modeling of the thermo-mechanical properties of carbon steels [J]. Acta Materialia, 2002, 50(9): 2259.

(Edited by PENG Chao-qun)